Modeling of Tissue Laser Irradiation in Cylindrical Coordinates Using the Finite Pointset Method

Anna KORCZAK[1)*], Felix R. SAUCEDO-ZENDEJO[2)]

[1)] *Silesian University of Technology, Faculty of Mechanical Engineering, Department of Computational Mechanics and Engineering, Gliwice, Poland*

[2)] *Universidad Autónoma de Coahuila, Centro de Investigacion en Matemáticas Aplicadas, Saltillo, México; e-mail: fesaucedoz@uadec.edu.mx*

[*] *Corresponding Author e-mail: anna.korczak@polsl.pl*

This study focuses on a numerical analysis of heat transfer in biological tissue. The proposed model is formulated using the Pennes equation under transient conditions within a two-dimensional (2D) cylindrical domain. The tissue undergoes laser irradiation, with internal heat sources determined based on the Beer–Lambert law. Moreover, key parameters, including the perfusion rate and effective scattering coefficient, are modeled as functions dependent on tissue damage. Numerical computations are performed using the finite pointset method (FPM). The findings, discussed in the final section, indicate that the FPM approach is a viable and effective tool for analyzing thermal processes in biological tissues.

Keywords: meshless methods, bioheat transfer, cylindrical system, FPM.

1. Introduction

This research investigates the use of the finite pointset method (FPM) to analyze heat transfer in biological tissues, building upon previous developments of a one-dimensional model [1]. The approach is based on the transient, two-dimensional (2D) Pennes equation formulated in a cylindrical coordinate system. A central focus of the study is the impact of laser irradiation, which is modeled using the Beer–Lambert law to characterize the attenuation of laser energy as it penetrates tissue. Understanding this process is essential for determining how laser energy is absorbed and transformed into heat. This knowledge is particularly relevant in medical applications, including laser-based therapies, oncology treatments, and surgical procedures. With the growing role of laser technology in healthcare, a deeper understanding of these mechanisms is necessary to enhance its precision and efficiency. The proposed model also considers

how tissue damage affects physiological parameters such as perfusion rate and effective scattering coefficient, acknowledging the dynamic changes in blood flow and tissue properties resulting from thermal exposure.

The FPM method is a truly meshfree technique, as it does not require the construction of structured or background meshes, unlike conventional methods such as the finite element method or finite difference method, to approximate the solution to an elliptic partial differential equation or to interpolate field variables [1]. In contrast, FPM employs a set of nodes scattered over the problem domain and its boundaries, combined with a weighted least-squares technique to construct local approximations [2]. Its Lagrangian formulation makes it especially well-suited for problems with highly complex geometries and irregular boundaries, while its strong form makes the imposition of boundary conditions very easy compared to other numerical techniques. For all these reasons, the FPM has been successfully developed and applied to problems involving fluid mechanics [3, 4], heat transfer [5], linear elasticity [6], piezoelectricity [7], and biharmonic equations governing thin plate bending or viscous fluid flow [8], among others. However, in all these previous developments, the FPM was proposed and formulated using Cartesian coordinates. Therefore, this manuscript presents, for the first time in the scientific literature to the best of the authors' knowledge, the pioneering development of the FPM in cylindrical coordinates and its application to modeling tissue subjected to laser irradiation.

The Pennes bioheat partial differential equation, along with its suitable boundary conditions, serves as a mathematical framework employed for describing the temperature distribution within biological tissues subjected to diverse heat sources, such as laser irradiation.

The Pennes equation in 2D Cartesian coordinates is given as follows [10]:

$$c\frac{\partial T}{\partial t}(x,y,t) = \lambda\left(\frac{\partial^2 T}{\partial x^2}(x,y,t) + \frac{\partial^2 T}{\partial y^2}(x,y,t)\right) + Q(x,y,t), \qquad (1)$$

where λ [W·m^{-1}·K^{-1}] is the thermal conductivity, c [J·m^{-3}·K^{-1}] is the volumetric specific heat, Q [W·m^{-3}] is the heat source, T [°C] is the temperature, t [s] is time, and x, y [m] denote spatial coordinates.

The domain sample considered in this study is defined in cylindrical coordinate system (Fig. 1); therefore, the heat transfer equation takes the following form:

$$c\frac{\partial T}{\partial t}(r,z,t) = \lambda\frac{1}{r}\left(\frac{\partial T}{\partial r}(r,z,t) + r\frac{\partial^2 T}{\partial r^2}(r,z,t)\right)$$
$$+ \lambda\frac{\partial^2 T}{\partial z^2}(r,z,t) + Q(r,z,t), \qquad (2)$$

where r, z are the geometric coordinates of the cylindrical coordinate system.
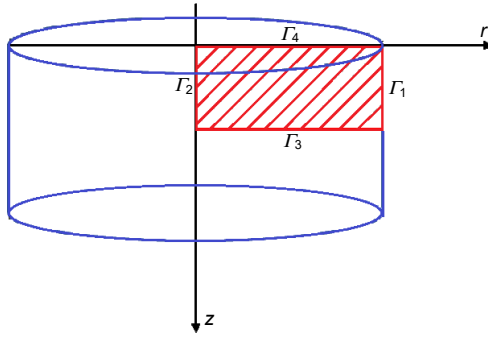
FIG. 1. Modeled sample with the considered domain and boundary.

The internal heat source is the sum of three components: heat generated by blood perfusion, metabolic heat production, and the absorption of heat from external sources:

$$Q(r, z, t) = Q_{\mathrm{perf}}(r, z, t) + Q_{\mathrm{met}} + Q_{\mathrm{las}}(r, z, t), \tag{3}$$

where Q_{perf}, Q_{met}, Q_{las} $[\mathrm{W \cdot m^{-3}}]$ are the heat sources due to perfusion, metabolism, and laser irradiation, respectively.

The laser heat source under analysis is described using Beer's law [11]:

$$Q_{\mathrm{las}}(r, z, t) = \mu'_t I_0 \exp\left(-\mu'_t z\right) \exp\left(-\frac{2r^2}{r_B^2}\right) s(t), \tag{4}$$

where I_0 $[\mathrm{W \cdot m^{-2}}]$ is the surface irradiance of the laser, r_B [m] is the radius of a laser beam, and $s(t)$ is a function equal to 1 when the laser is on and 0 when the laser is off, whereas μ'_t $[\mathrm{m^{-1}}]$ denotes the attenuation coefficient defined as [12]:

$$\mu'_t = \mu_a + \mu'_s, \tag{5}$$

where μ_a $[\mathrm{m^{-1}}]$ is the absorption coefficient and μ'_s $[\mathrm{m^{-1}}]$ is the effective scattering coefficient, which may can be considered either as a fixed value or as a function dependent on the Arrhenius damage integral:

$$\mu'_s(\theta) = \mu'_{s\,\mathrm{nat}} \exp\left(-\theta\right) + \mu'_{s\,\mathrm{den}} \left(1 - \exp\left(-\theta\right)\right). \tag{6}$$

The Arrhenius integral is defined as follows [10]:

$$\theta(r, z, t) = \int\limits_0^t A \exp\left[-\frac{\Delta E}{RT\left(r, z, \widehat{t}\right)}\right] d\widehat{t}, \tag{7}$$

where A [s^{-1}] is the pre-exponential factor, ΔE [J$\cdot$mol^{-1}] is the activation energy of the reaction R [J$\cdot$mol$^{-1}\cdot$K^{-1}] that is the universal gas constant (the values of parameters can be seen in Table 1).

TABLE 1. Arrhenius injury integral parameters [18, 19].

Symbol	Parameter	Value	Unit
A	Pre-exponential factor	$3.1\cdot 10^{98}$	s^{-1}
ΔE	Activation energy	$6.27\cdot 10^{5}$	J$\cdot$mol^{-1}
R	Universal gas constant	8.314	J$\cdot$mol$^{-1}\cdot$K^{-1}

The perfusion heat source function is considered as follows:

$$Q_{\text{perf}}(r, z, t) = c_B G_B(r, z, t)\left(T_B - T(r, z, t)\right), \tag{8}$$

where G_B [m$^3_{\text{blood}}\cdot$s$^{-1}\cdot$m$^{-3}_{\text{tissue}}$] is the blood perfusion rate, c_B [J$\cdot$m$^{-3}\cdot$K^{-1}] is the volumetric specific heat of blood, and T_B [$^\circ$C] denotes the arterial blood temperature. Additionally, the blood perfusion coefficient is a function of the tissue's necrotic alterations [10]:

$$G_B\left(\theta(r, z, t)\right) = G_{B0}w\left(\theta(r, z, t)\right), \tag{9}$$

where G_{B0} represents the initial perfusion rate, and we assume that function w follows a polynomial form [10]:

$$w\left(\theta(r, z, t)\right) = \sum_{j=1}^{3} m_j\theta(r, z, t)^{j-1}, \tag{10}$$

where m_j are fixed coefficients (Table 2).

TABLE 2. Coefficients of the perfusion coefficient function [10, 19].

θ	m_1	m_2	m_3
$\theta = 0$	1	0	0
$0 < \theta \leq 0.1$	1	25	-260
$0.1 < \theta \leq 1$	1	-1	0
$\theta > 1$	0	0	0

Moreover, Eq. (2) should be supplemented by boundary and initial conditions. The analyzed model, in the first numerical example, is complemented by the following boundary conditions:

$$(r, z) \in \varGamma_i : -\lambda\frac{\partial T}{\partial n_0}(r, z, t) = 0, \qquad i = 1, 2, 3, \tag{11}$$

$$(r, z) \in \Gamma_4 : -\lambda \frac{\partial T}{\partial n_0}(r, z, t) = q_b(r, z, t), \tag{12}$$

where T_b and q_b are the boundary temperature and heat flux, respectively. In the second numerical example, the third type of boundary condition applied on the irradiated surface is considered:

$$-\lambda \frac{\partial T}{\partial n_0} = \alpha \left(T(r, z, t) - T_{\text{amb}} \right), \tag{13}$$

where n_0 [m] is the outward normal vector ($n_0 = [n_x, n_y]$) and T_{amb} is the ambient temperature. The initial temperature distribution is considered to be constant T_0 [°C].

The Pennes equation presented must be solved numerically to estimate the temperature distribution. This article proposes using the FPM, which is explained in detail in Sec. 2.

2. Finite pointset method

The FPM is a meshfree Lagrangian approach that employs a weighted least-squares interpolation technique to estimate spatial derivatives and solve partial differential equations [13]. The FPM uses Taylor series to calculate function values and their derivatives, where the unknown coefficients in the series naturally correspond to the function derivatives. A more comprehensive guide on applying the classical version of the FPM can be found in various literature sources [2, 13–16]. In this section, we will outline the fundamental concept of the FPM as specifically applied to the Pennes equation in cylindrical coordinates.

First, the main idea of the FPM needs to be explained. For this purpose let us consider a domain X with a defined boundary. Within this domain X, we have a collection of n points $x_1, x_2, ..., x_n$ ($x_j = [x_j^1, x_j^2]$, $j = 1, ..., n$), each associated with respective function values $T(x_1), T(x_2), ..., T(x_n)$. The objective is to approximate the value of T at an arbitrary location x ($x = [x^1, x^2]$). To achieve this, we define the approximation of $f(x_j)$ using a Taylor series expansion ($dx_j^k = x_j^k - x^k$, $k = 1, 2$) centered around x:

$$\widetilde{T}(x_j) = T(x) + \sum_{k=1}^{2} T_k(x) dx_j^k + \frac{1}{2} \sum_{k,l=1}^{2} T_{kl}(x) dx_j^k dx_j^l. \tag{14}$$

The values $T(x)$, $T_k(x)$, $T_{kl}(x)$, ($k = 1, 2$, $l = 1, 2$) are the unknowns to be determined using a weighted least-squares method. This method minimizes the following quadratic expression over all neighboring points (np):

$$J = \sum_{j=1}^{np} w_j (\mathbf{Ma} - \mathbf{b})^2, \tag{15}$$

where $w_j = w(x_j, x)$ and

$$
w(x_j, x) = \begin{cases} \exp\left(-\beta \left\| x_j - x \right\|^2 / h^2\right), & \left\| x_j - x \right\| \le h, \\ 0, & \text{otherwise,} \end{cases} \tag{16}
$$

where β is a positive constant. The value h is the radius that defines a set of neighboring points around x.

Equation (15) can be expressed in the following form:

$$
J = (\mathbf{Ma} - \mathbf{b})^T \mathbf{W}(\mathbf{Ma} - \mathbf{b}), \tag{17}
$$

where

$$
\mathbf{W} = \begin{pmatrix} w\left(x_1, x\right) & 0 & \cdots & 0 \\ 0 & w\left(x_2, x\right) & 0 & 0 \\ \vdots & \vdots & \ddots & \vdots \\ 0 & 0 & \cdots & w\left(x_{np}, x\right) \end{pmatrix}. \tag{18}
$$

Formally, the minimization of the function J results in:

$$
\mathbf{a} = (\mathbf{M}^T \mathbf{W} \mathbf{M})^{-1}(\mathbf{M}^T \mathbf{W})\mathbf{b}. \tag{19}
$$

At this stage, we assume that x lies in the interior part of X. Moreover, the matrix $\mathbf{M}$, constructed taking into account the Pennes equation (2) (Δt is the time step), which must be satisfied at these interior points, is defined as follows:

$$
\mathbf{M} = \begin{pmatrix} 1 & \Delta x_1^1 & \Delta x_1^2 & \frac{1}{2}\left(\Delta x_1^1\right)^2 & \Delta x_1^1 \Delta x_1^2 & \frac{1}{2}\left(\Delta x_1^2\right)^2 \\ 1 & \Delta x_2^1 & \Delta x_2^2 & \frac{1}{2}\left(\Delta x_2^1\right)^2 & \Delta x_2^1 \Delta x_2^2 & \frac{1}{2}\left(\Delta x_2^2\right)^2 \\ \vdots & \vdots & \vdots & \vdots & \vdots & \vdots \\ 1 & \Delta x_{np}^1 & \Delta x_{np}^2 & \frac{1}{2}\left(\Delta x_{np}^1\right)^2 & \Delta x_{np}^1 \Delta x_{np}^2 & \frac{1}{2}\left(\Delta x_{np}^2\right)^2 \\ 2c & -2\Delta t\lambda \frac{1}{x^1} & 0 & -\Delta t\lambda & 0 & -\Delta t\lambda \end{pmatrix}. \tag{20}
$$

Then, $\mathbf{a}$ and $\mathbf{b}$ take the following forms (τ is the time index):

$$
\mathbf{a} = [T(x), T_1(x), T_2(x), T_{11}(x), T_{12}(x), T_{22}(x)]^T, \tag{21}
$$

$$
\mathbf{b} = \left[T^{\tau+1}(x_1), T^{\tau+1}(x_2), ..., T^{\tau+1}(x_{np}), 2\Delta t Q^\tau \right.
$$
$$
\left. + 2cT^\tau(x) + \lambda \Delta t \nabla^2 T^\tau(x)\right]^T. \tag{22}
$$

Additionally, the FPM operates iteratively where the vector $\mathbf{a}$ is updated for each particle using Eq. (19). The algorithm applied includes a stopping criterion based on the relative error, defined as follows:

$$\frac{\sum\limits_{j=1}^{np} \left| T^{l+1,\tau}(x_j,t) - T^{l,\tau}(x_j,t) \right|}{\sum\limits_{j=1}^{np} \left| T^{l+1,\tau}(x_j,t) \right|} < \varepsilon, \tag{23}$$

where l is the iteration counter, and ε is the maximum relative error.

It is worth mentioning that if point x belongs to the boundary of X and satisfies the second type of boundary condition, one additional row must be added to matrix (20): $[0, n_x, n_y, 0, 0, 0]$ and an additional element must be added to vector (22): $\frac{-q_b}{\lambda}$, because we have one more equation to consider. For the third boundary condition, we have $[\alpha/\lambda, n_x, n_y, 0, 0, 0]$ and $\alpha T_{\mathrm{amb}}/\lambda$, respectively.

3. Results and discussion

The study concludes by presenting the results obtained from numerical calculations. Two numerical examples, each with two different sets of input data, are proposed. To assess the feasibility of the proposed computational technique, the first benchmark example is considered, which is independent of the injury integral parameters shown in Table 1. The relevant thermo-optical parameters for this example are presented in Table 3. The numerical results of this example are compared with reference numerical results published in the literature.

TABLE 3. Thermo-optical parameters [17].

Symbol	Parameter	Value	Unit
λ	Thermal conductivity of tissue	0.445	$\mathrm{W \cdot m^{-1} \cdot K^{-1}}$
c	Volumetric specific heat of tissue	3.96	$\mathrm{MJ \cdot m^{-3} \cdot K^{-1}}$
G_B	Blood perfusion coefficient	0.00125	$\mathrm{s^{-1}}$
Q_{met}	Metabolic heat source	245	$\mathrm{W \cdot m^{-3}}$
c_B	Volumetric specific heat of blood	3.9962	$\mathrm{MJ \cdot m^{-3} \cdot K^{-1}}$
T_B	Arterial blood temperature	37	$^\circ\mathrm{C}$

In this first example, the simulation involving irradiation modeled by applying a heat flux as a boundary condition is analyzed. The external heat flux is assumed to have the form of a Gauss-type function [17]:

$$q_b(r,0,t) = q_0 \exp\left[-\frac{r^2}{2(R/3)^2} \right]. \tag{24}$$

In the dermis tissue region with dimensions: 12 mm depth (d) and 20 mm radius (R), the location of points is considered as a regular structure and is generated with a spatial step $\Delta r = \Delta z = 1$ mm. The time step Δt is set to 0.01 sec. In the FPM, the sampling density is usually controlled with the definition of the mean minimum distance between points $h_0 = \frac{1}{n} \sum_{i=1}^{n} \min\{\Delta r, \Delta z\}$, which in turn is linked to h through the formula $h = C_h h_0$. The value of C_h providing the lowest numerical error was studied previously and it was found to be around 3 [7]. Therefore, the radius used to determine neighboring points in the FPM for this study was fixed as $h = 3h_0$, as this ensured that the system of equations (19) is solvable, has a sufficient number of neighboring points without being overdetermined, and results in minimal numerical error, as reported in [7]. The parameter β ($\beta = 6$) in Eq. (16) can be freely chosen in FPM (already investigated in [7]). The value q_0 is assumed to be 2 kW$\cdot$m^{-2}, as in [17], and the time of irradiation is 5.211 seconds.

As it can be seen in Fig. 2, the comparison between the results obtained using the interval finite difference method in [17] and those from FPM shows that the computed single-valued temperatures are in a good agreement and fall within the expected temperature intervals.
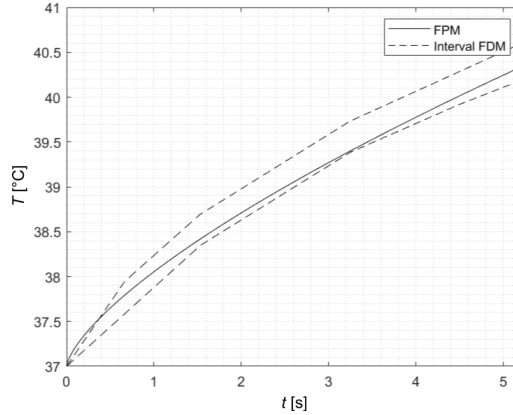

FIG. 2. Profiles of skin surface temperature at $r = 0$.

The second numerical example examines the Pennes equation with parameters such as the perfusion rate and the effective scattering coefficient, which are influenced by tissue damage outcomes. The model under consideration is enhanced by applying a third-type boundary condition on the tissue surface exposed to laser irradiation, while adiabatic conditions are assumed on the remaining boundaries [18]. For the third-type boundary condition, the following input data are considered [18]: $\alpha = 10$ W$\cdot$m$^{-2}\cdot$K^{-1} (convective heat transfer coefficient) and $T_{\mathrm{amb}} = 20°$C (ambient temperature).

The initial temperature in all the points is assumed as a constant value $T_0 = 37°C$. The peak power laser intensity is considered as $I_0 = 30$ kW $\cdot$ m^{-2}. The assumed thermo-optical parameters of the tissue are presented in Table 4, while the Arrhenius injury integral parameters can be found in Table 1. The coefficients used in the w function (7) are listed in Table 2. It is worth noting that the optical parameters used here are typical for near-infrared radiation on soft tissue, such as with a Nd:YAG laser operating at 1064 nm. During coagulation in this type of laser-tissue interaction, the reduced scattering coefficient may increase by 3–4 times its original value (i.e., the effective scattering coefficient of native tissue), while the absorption coefficient remains constant [11].

TABLE 4. Thermo-optical parameters [18].

Symbol	Parameter	Value	Unit
λ	Thermal conductivity of tissue	0.609	W $\cdot$ m^{-1} $\cdot$ K^{-1}
c	Volumetric specific heat of tissue	4.18	MJ $\cdot$ m^{-3} $\cdot$ K^{-1}
G_{B0}	Initial blood perfusion coefficient	0.00125	s^{-1}
μ_a	Absorption coefficient of tissue	40	m^{-1}
$\mu'_{s\,\text{nat}}$	Effective scattering coefficient of native tissue	1000	m^{-1}
$\mu'_{s\,\text{den}}$	Effective scattering coefficient of destructed tissue	4000	m^{-1}
Q_{met}	Metabolic heat source	245	W $\cdot$ m^{-3}
c_B	Volumetric specific heat of blood	3.9962	MJ $\cdot$ m^{-3} $\cdot$ K^{-1}
T_B	Arterial blood temperature	37	°C

The numerical computations were performed at three selected depths: 0, 1, and 1.5 mm, located along the main optical path of the laser beam. The time of irradiation was set to 10 seconds. The stopping criterion (23) was applied with $\varepsilon = 10^{-4}$. As in the previous numerical example, the results obtained by the FPM match very well those obtained by Jasiński [18], who used the boundary element method (BEM) for the central point on the skin surface. This is shown in Fig. 3. Some acceptable differences (not exceeding 2°C at 0 mm depth, corresponding to an error of 3.63%) between FPM and BEM can be observed, which are due to the fact that in [18], the author constructed the solutions for a classical 2D case using Cartesian coordinates.

Moreover, calculations were performed for other parameters including the injury integral, laser heat source intensity, perfusion coefficient, and effective scattering coefficient (Figs. 4a–d). In these figures, the influence of the injury integral on these parameters is evident, especially at $z = 0$, where, after 6.8 s, the injury integral reaches a maximum value of 1.
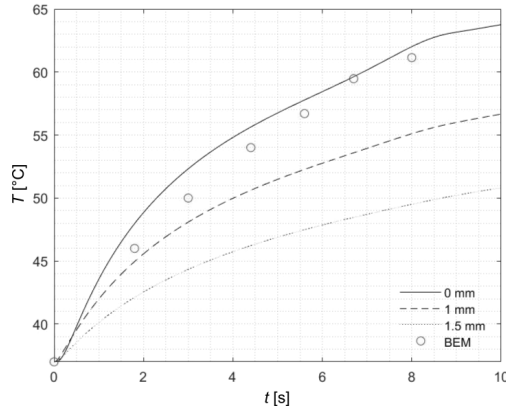
FIG. 3. Temperature profiles in three different points within the domain
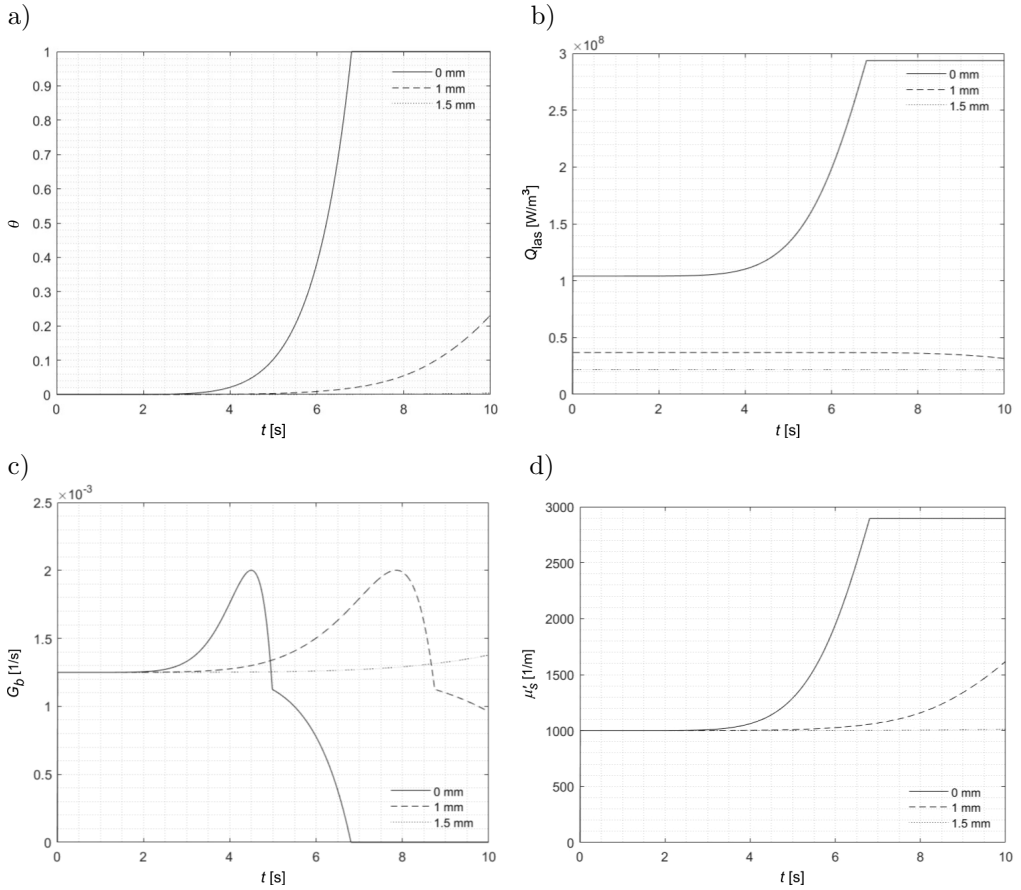for depths $z = 0$, 1, and 1.5 mm.

FIG. 4. Temporal profiles of: a) the injury integral, b) the laser heat source intensity, c) the
perfusion coefficient, and d) the effective scattering coefficient at three different points of
the domain for depths $z = 0$, 1, and 1.5 mm.

4. Conclusion

A novel FPM approach formulated in cylindrical coordinates for the analysis of transient bioheat transfer problems was presented for the first time in this article. For the assessment of this numerical technique, the considered bioheat transfer problems were modeled by Pennes' equation in cylindrical coordinates. Based on the reported numerical results and the excellent agreement with the corresponding numerical solutions, available in the literature, used as benchmark examples, it can be concluded that this meshfree numerical formulation is suitable for solving complex problems involving temperature- and necrosis-dependent parameters. The straightforward and effective incorporation of the corresponding boundary conditions enhances its computational implementation in potential applications in multi-layered or 3D scenarios.

Due to all these features, its good numerical behavior and the efficient, stable manner in which the numerical examples were successfully solved, it can be concluded that this novel approach is a promising numerical tool for modeling nonlinear dynamic thermal processes in biological tissue exposed to laser irradiation. Moreover, it can also be extended to other bioheat transfer formulations, such as the Cattaneo–Vernotte equation [20] or the dual-phase lag equation [21], which makes it of particular interest for future research.

Acknowledgements

References

1. A. Korczak, Numerical modeling of tissue laser irradiation with uncertain parameters using the interval finite pointset method, *Journal of Applied Mathematics and Computational Mechanics*, **23**(2): 41–53, 2024, https://doi.org/10.17512/jamcm.2024.2.04.

2. J. Kuhnert, *General Smoothed Particle Hydrodynamics*, Ph.D. thesis, Technische Universität Kaiserslautern, 1999.

3. S. Tiwari, A. Klar, G. Russo, Modelling and simulations of moving droplet in a rarefied gas, *International Journal of Computational Fluid Dynamics*, **35**(8): 666–684, 2021, https://doi.org/10.1080/10618562.2021.2024520.

4. C. Drumm, S. Tiwari, J. Kuhnert, H.J. Bart, Finite pointset method for simulation of the liquid–liquid flow field in an extractor, *Computers & Chemical Engineering*, **32**(12): 2946–2957, 2008, https://doi.org/10.1016/j.compchemeng.2008.03.009.

5. F.R. Saucedo-Zendejo, J.M. Nóbrega, A novel approach to model the flow of generalized Newtonian fluids with the finite pointset method, *Computational Particle Mechanics*, **9**: 585–595, 2022, https://doi.org/10.1007/s40571-021-00432-y.

6. E.O. Reséndiz-Flores, F.R. Saucedo-Zendejo, Two-dimensional numerical simulation of heat transfer with moving heat source in welding using the finite pointset method, *International Journal of Heat and Mass Transfer*, **90**: 239–245, 2015, https://doi.org/10.1016/j.ijheatmasstransfer.2015.06.023.

7. F.R. Saucedo-Zendejo, A novel meshfree approach based on the finite pointset method for linear elasticity problems, *Engineering Analysis with Boundary Elements*, **136**: 172–185, 2022, https://doi.org/10.1016/j.enganabound.2021.12.011.

8. L.J.T. Doss, N. Kousalya, Finite pointset method for biharmonic equations, *Computers and Mathematics with Applications*, **75**(10): 3756–3785, 2018, https://doi.org/10.1016/j.camwa.2018.02.029.

9. F.R. Saucedo-Zendejo, J.L. Medrano-Mendieta, A.G. Nuñez-Briones, A GFDM approach based on the finite pointset method for two-dimensional piezoelectric problems, *Engineering Analysis with Boundary Elements*, **163**: 12–22, 2024, https://doi.org/10.1016/j.enganabound.2024.02.014.

10. J.P. Abraham, E.M. Sparrow, A thermal-ablation bioheat model including liquid-to-vapor phase change, pressure- and necrosis-dependent perfusion, and moisture-dependent properties, *International Journal of Heat and Mass Transfer*, **50**(13–14): 2537–2544, 2007, https://doi.org/10.1016/j.ijheatmasstransfer.2006.11.045.

11. T.N. Glenn, S. Rastegar, S.L. Jacques, Finite element analysis of temperature controlled coagulation in laser irradiated tissue, *IEEE Transactions on Biomedical Engineering*, **43**(1): 79, 1996, https://doi.org/10.1109/10.477703.

12. M.H. Niemz, *Laser-Tissue Interaction*, Springer, Berlin, Heidelberg, New York, 2007, https://doi.org/10.1007/978-3-030-11917-1.

13. J. Kuhnert, S. Tiwari, Grid free method for solving the Poisson equation, *Berichte des Fraunhofer ITWM*, Nr. 25, Fraunhofer-Institut für Techno- und Wirtschaftsmathematik ITWM, Kaiserslautern, 2001.

14. F.R. Saucedo-Zendejo, E.O. Reséndiz-Flores, Meshfree numerical approach based on the finite pointset method for two-way coupled transient linear thermoelasticity, *Computational Particle Mechanics*, **10**(2): 289–302, 2023, https://doi.org/10.1007/s40571-022-00496-4.

15. A. Wawreńczuk, J. Kuhnert, N. Siedow, FPM computations of glass cooling with radiation, *Computer Methods in Applied Mechanics and Engineering*, **196**(45–48): 4656–4671, 2007, https://doi.org/10.1016/j.cma.2007.05.025.

16. F.R. Saucedo-Zendejo, E.O. Reséndiz-Flores, Meshfree numerical approach based on the Finite Pointset Method for static linear elasticity problems, *Computer Methods in Applied Mechanics and Engineering*, **372**: 113367, 2020, https://doi.org/10.1016/j.cma.2020.113367.

17. B. Mochnacki, A. Piasecka Belkhayat, Numerical modeling of skin tissue heating using the interval finite difference method, *Molecular & Cellular Biomechanics*, **10**(3): 233–244, 2013, https://doi.org/10.3970/mcb.2013.010.233.

18. M. Jasiński, Modelling of thermal damage in laser irradiated tissue, *Journal of Applied Mathematics and Computational Mechanics*, **14**(4): 67–78, 2015, https://doi.org/10.17512/jamcm.2015.4.07.

19. M. Jasiński, Numerical modeling of tissue coagulation during laser irradiation controlled by surface temperature, *Scientific Research of the Institute of Mathematics and Computer Science*, **9**(1): 29–36, 2010.

20. E. Majchrzak, G. Kałuża, J. Poteralska, Application of the DRBEM for numerical solution of Cattaneo-Vernotte bioheat transfer equation, *Scientific Research of the Institute of Mathematics and Computer Science*, **7**(1): 111–120, 2008.

21. B. Partovi, H. Ahmadikia, M. Mosharaf-Dehkordi, Analytical and numerical analysis of the dual-pulse lag heat transfer in a three-dimensional tissue subjected to a moving multi-point laser beam, *Journal of Thermal Biology*, **112**: 103431, 2023, https://doi.org/10.1016/j.jtherbio.2022.103431.